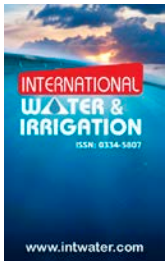

International Water and Irrigation
Volume 43 Issue 2, (2024)
ISSN: 0334-5807
Pages 82 - 96

Effect verification in ecological landscape design of riverbank leisure space based on sketch line simulation analysis

Haoyu Li[1,3], Yunhui Zhang[2,*]

[1]School of agriculture and water conservancy project ,Suihua University , Suihua,Heilongjiang ,152000, China

[2]School of Economics and Management,Suihua University , Suihua,Heilongjiang ,152000, China

[3]School of Horticulture and Landscape Architecture, Jinling Institute of Technology, Nanjing , 210038 , China

* Corresponding author: Yunhui Zhang

Abstract. In order to improve the effectiveness of landscape design for riverbank leisure spaces, this article applies sketch line simulation technology to the design of leisure space landscapes, constructs a design model suitable for the needs of modern urban leisure space landscapes near rivers, and automatically generates high fidelity wireframes through hand drawn user interface sketches, thereby improving the efficiency of prototype design. The key to automatically generating high fidelity wireframes is to accurately detect the type and position of UI components from hand drawn UI sketches. In addition, a prototype software tool plugin was implemented to detect hand drawn UI sketches using an improved Faster R CNN and automatically convert the detection results into high fidelity wireframes. Through computer simulation research, we can see that sketch line simulation has a good effect in the landscape design of leisure spaces near riverbanks in cities.

Keywords: sketch; Line simulation; Leisure space; Landscape design, riverbank.

1 INTRODUCTION

The concept of graphics engine can be summarized as an organic combination of codes in various graphics applications. This combination is not a simple concentration and combination of application codes. It summarizes and abstracts the similar program structures and functional requirements in various graphics applications, and realizes and encapsulates these functions with appropriate structures and modules, thus forming a general graphics application framework independent of external resources and the underlying graphics API function set. The industrial term "engine" is a good illustration of the role of this framework and its relationship with graphics applications. Today, when graphics engines are widely used, the processing capacity of a graphics engine directly determines the quality of graphics applications developed on its architecture.

The technical characteristics of graphic engines essentially refer to the implementation and encapsulation of various common functions in graphic application software within its architecture, so that when developing graphic applications on it, these functions can be directly called to reduce coding workload and shorten development cycle [1].

In a complex scene, there is often a large number of scene elements. In order to improve rendering efficiency, graphics engines usually use a certain cropping algorithm to only render objects visible within the camera range.

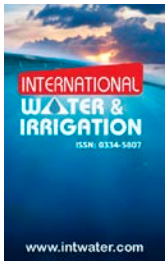

International Water and Irrigation
Volume 43 Issue 2, (2024)
ISSN: 0334-5807
Pages 82 - 96

All invisible objects will be directly discarded to prevent them from occupying precious video memory and bandwidth resources of the graphics card[2].

Lighting and shadows are one of the elements that make up a scene, and good lighting and shadow rendering provides a large amount of material and depth information for the scene, which is an indispensable part of pursuing realistic rendering of the scene. Due to the limitations of the current hardware system, support for lighting can only be limited to image based lighting such as local lighting and HDR. Currently, more advanced graphics engines can provide direct support for fuzzy shadow algorithms [3].

Terrain rendering is the foundation of outdoor scene rendering, and providing support and simplified algorithms for large-scale terrain rendering is an important responsibility of graphic engines for outdoor scene rendering applications. There are many algorithms currently used for terrain rendering, which can be roughly divided into LOD related terrain simplification, terrain data scheduling strategies, and terrain special effects, such as surface deformation, dynamic terrain, etc. [4-5].

It is precisely because of the research and implementation of various special effects technologies that the graphic applications of games and movies are so popular. Imagine that without the stunning explosion effect, bizarre spell details, and screen effects such as water droplets and blood stains, various applications would lose a lot of color. The example system is one of the basic support of graphics engines for special effects technology, and it has also become a standard support for various graphics engines. With the research in this area, various special effects technologies have also been adopted and directly supported by graphics engines.

Some technologies supported by graphics engines that are not closely related to graphics rendering. These technologies include basic mathematical library support, memory management support, physical computing support, and logical support for multi role and multi task. Although these technologies are not closely related to rendering, they still occupy a core position in graphics engines and are supported by a large number of graphics engines [6]

Image based tree modeling refers to the use of images (sequences) to calculate and predict the depth information of tree branches through reasonable modeling and optimization, as well as to restore the branch information of occluded parts. Unlike manual modeling, image-based tree modeling can directly generate a 3D model of a tree from a single image or multiple images. The biggest advantage of this method is that it can obtain a Tree model with high precision and strong realism, which is generally proportional to the resolution of the image used [7]. Reference [8] proposes an image based semi-automatic modeling method for broad-leaved shrubs. This method first utilizes SfM (Structure from Motion) technology to obtain three-dimensional structural information of plants, then segments and restores the leaves of clearly distinguishable broad-leaved shrubs, and finally restores the structure of the branches through interactive methods. The method proposed in reference can reconstruct trees and their small leaves. This method first automatically reconstructs the visible branches based on the image, and then completes the modeling of the obstructed branches by referencing and copying the reconstructed branch structure as a template. For the leaves, they are first segmented from the input image, filtered and mapped directly onto the branches, achieving the modeling of the tree. Reference proposed an interactive tree reconstruction method based on sparse images, which only requires taking two tree photos with a 90 degree

International Water and Irrigation
Volume 43 Issue 2, (2024)
ISSN: 0334-5807
Pages 82 - 96

difference and 4-7 intermediate photos. The method combines interactive editing with branch structure extraction, perspective correction, and leaf generation algorithms to reconstruct a highly realistic 3D model of the tree.

This paper applies sketch line simulation technology to leisure space landscape design, constructs a design model suitable for modern urban leisure space landscape and analyzes its design effect, so as to improve the scientific nature of leisure landscape design.

2 SKETCH DETECTION OF HAND-DRAWN UI BASED ON FASTERR-CNN

This paper introduces a sketch data enhancement technique based on Bezier Pivot based deformation (BPD), and then introduces the hand-drawn UI sketch data set ImageCLEF drawn UI and the process of building UI sketch component data set for training ResNet network.

Data enhancement technology plays a very important role in the field of computer vision. Usually, the number of training samples is increased by simply transforming the original data set images (such as translation, rotation, flip and scaling). However, the diversity obtained by this modification of images is relatively small, and correlation is introduced into the training data. Therefore, this paper introduces a BPD strategy to enrich training data.

For a hand-drawn sketch S, this method first converts it into a gray image, and then performs a simple threshold operation to obtain a binary image B. In order to extract the center line S 'of sketch, the skeletonization method based on morphology is applied to B. Specifically, it is to continuously etch the pixels on the boundary of the object in the binary image, but in the process of etching, it is necessary to ensure that the points that meet certain conditions are retained or deleted, so as to determine that only one pixel wide image remains after etching. Then, S' is divided into several disjoint square blocks with a × a size. For sketches of 256 × 256 size, this paper sets a = 32. Considering the thickness of the line in the sketch, the center line is extracted before segmentation, which can avoid a short part of the line being divided into two small blocks. In each small block, the largest connected pixel set is selected as the main curve T, which is fitted by a cubic Bessel curve, and the curve containing only a few pixels will be eliminated to ensure the fitting performance.

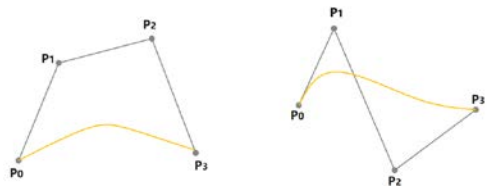

Figure 1 Illustration of cubic Bessel curve

P0 and P3 are the starting and ending points respectively, and P1 and P2 are the intermediate control pivots. There are only four control pivots, which can represent a rich variety of curves.

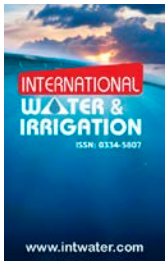

International Water and Irrigation
Volume 43 Issue 2, (2024)
ISSN: 0334-5807
Pages 82 - 96

Cubic Bessel curve can model different curves through four control axes. As shown in Figure 1, if the coordinates of the control pivot are changed, a series of points can be obtained, which form a new curve. The function of the cubic Bessel curve is as follows:

$$f = (1-t)^3 P_0 + 3t(1-t)^2 P_1 + 3t^2(1-t)P_2 + t^3 P_3 \quad (1)$$

Among them, $t \in [0,1], P_0$ and P_3 are the starting point and the ending point of the curve respectively. Pivots P_1 and P_2 are the control point, which determines the bending shape. For simpler representation, $\phi = 1-t$ is introduced to simplify the formula, so as to obtain:

$$f = \phi^3 P_0 + 3t\phi^2 P_1 + 3t^2\phi P_2 + t^3 P_3 \quad (2)$$

The goal of BPD is to generate more diversified sketches by controlling the pivot to deform sketch squares based on these Bessel curves. For the curve T in each sketch box, P_0 and P_3 can be obtained directly, and P_1 and P_2 need to be calculated. We assume that the curve T consists of n points, which is expressed as $v_i (i = 1,2,3,..,n)$, BPD suggests that the least square method should be used to find the best fit Bessel curve. The objective function is defined as:

$$f^* = \min L = \min \sum_{i=1}^{n} \left(v_i - f\left(t_i\right) \right)^2 \quad (3)$$

By minimizing the objective function, we can get the curve function f, which can be solved by calculating the partial derivative of L with respect to P_1 and P_2, and the formula is as follows:

$$\frac{\partial L}{\partial P_1} = 0 \quad (4)$$

$$\frac{\partial L}{\partial P_2} = 0 \quad (5)$$

By substituting equation (2) into equation (4), we can get:

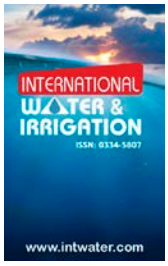

International Water and Irrigation
Volume 43 Issue 2, (2024)
ISSN: 0334-5807
Pages 82 - 96

$$\frac{\partial \sum_{i=1}^{n}\left(v_i-\phi_i^3P_0-3t_i\phi_i^2P_1-3t_i^2\phi_iP_2-t_i^3P_3\right)^2}{\partial \mathrm{p}_1}$$

$$=\sum_{i=1}^{n}2\left(v_i-\phi_i^3P_0-3t_i\phi_i^2P_1-3t_i^2\phi_iP_2-t_i^3P_3\right)\times\left(-3t_i\phi_i^2\right) \quad (6)$$

$$=\sum_{i=1}^{n}2\left(v_i-\phi_i^3P_0-t_i^3P_3\right)\times\left(-3t_i\phi_i^2\right)$$

$$+\sum_{i=1}^{n}2\left(9t_i^2\phi_i^4P_1+9t_i^3\phi_i^3P_2\right)=0$$

From the above equation, we can easily get:

$$\sum_{i=1}^{n}3t_i^2\phi_i^4P_1+\sum_{i=1}^{n}3t_i^3\phi_i^3P_2=\sum_{i=1}^{n}t_i\phi_i^2\left(v_i-\phi_i^3P_0-t_i^3P_3\right) \quad (7)$$

To simplify this formula, the custom symbol a_1、b_1 and c_1 are introduced to represent equation 7:

$$a_1=\sum_{i=1}^{n}3t_i^2\phi_i^4$$

$$b_1=\sum_{i=1}^{n}3t_i^3\phi_i^3 \quad (8)$$

$$c_1=\sum_{i=1}^{n}t_i\phi_i^2\left(v_i-\phi_i^3P_0-t_i^3P_3\right)$$

Thus, the equation can be written as:

$$a_1P_1+b_1P_2=c_1 \quad (9)$$

Moreover, we can derive from equation 5:

$$a_2P_1+b_2P_2=c_2 \quad (10)$$

The coefficients in equation 10 are defined as follows:

$$a_2=b_1=\sum_{i=1}^{n}3t_i^3\phi_i^3 \quad (11)$$

$$b_2=\sum_{i=1}^{n}3t_i^4\phi_i^2 \quad (12)$$

$$c_2=\sum_{i=1}^{n}t_i^2\phi_i\left(v_i-\phi_i^3P_0-t_i^3P_3\right) \quad (13)$$

International Water and Irrigation
Volume 43 Issue 2, (2024)
ISSN: 0334-5807
Pages 82 - 96

By replacing equation (10) with equation (9), the variable P_1 and P_2 is expressed as:

$$p_1 = \frac{b_2 c_1 - b_1 c_2}{a_1 b_2 - b_1 b_1}$$
$$p_2 = \frac{a_1 c_2 - b_1 c_1}{a_1 b_2 - b_1 b_1} \quad (14)$$

Due to the high abstractness of hand-drawn sketches and the differences in painting skills between people, the sketches drawn show great diversity in many aspects such as curve length and bending degree. Considering the large number of people and the difference of drawing skills, the change of hand-drawn sketch is closer to a random process. Therefore, BPD applies the random shift Δ to the obtained control pivot P to obtain the position of the new pivot P', as follows:

$$P' = P + \Delta \quad (15)$$

Among them, $\Delta = (x, y), x、\ y \in [-\alpha, \alpha], \alpha$ refers to the degree of deformation. In the experiment of this paper, we set $\alpha = 8$ for the sketch image of 256×256. Based on these new control pivots, the deformed sketch is moved by the least square algorithm.

FasterR-CNN is a region-based target detection algorithm, which locates candidate regions in advance and then identifies the classes of candidate regions. FasterR-CNN creatively proposed RPN to automatically generate target candidate regions. It avoids the redundancy of traditional detection algorithms to generate candidate regions, realizes the end-to-end training process, and greatly improves the accuracy and speed of detection.

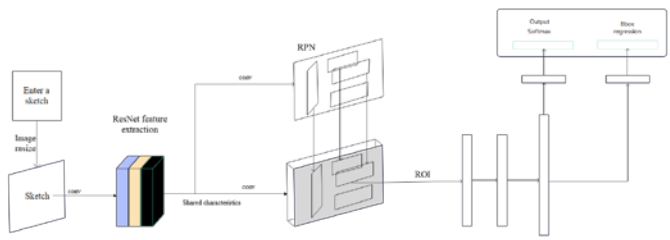

Figure 2 FasterR-CNN network structure

In this paper, ResNet-50 is used as the feature extraction network of FasterR-CNN model, and its network structure is shown in Figure 2.

International Water and Irrigation
Volume 43 Issue 2, (2024)
ISSN: 0334-5807
Pages 82 - 96

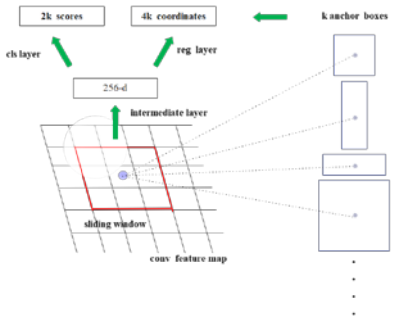

Figure 3 Schematic diagram of RPN network

The function of RPN network is to generate candidate regions, its input is the feature map output by the feature extraction network, and its output is all candidate boxes that may contain targets and the confidence that there are targets in the boxes. Figure 3 is a schematic diagram of RPN network principle. RPN network first uses a fixed size 3×3 convolution check to convolve the feature map, and its output tensor dimension is the same as that of the input feature map. When the convolution kernel is used to slide to each position on the feature map, the RPN network generates k anchor frames corresponding to the anchor points with different scales and widths.

According to the above definition, FasterR-CNN can define the loss function of RPN network as:

$$L(p,t)=\frac{1}{N\text{cs}}\sum_i L_{\text{ch}}(p,p_i^*)+\lambda\frac{1}{N\text{ag}}\sum_i p_i^* L_{\text{config}}(t_i,t_i^*)\ (16)$$

Among them, i represents the index value of an anchor box in the corresponding training batch, and p_i represents the probability that the network predicts whether the I-th anchor box has a detection target. p_i^* represents whether the i-th anchor box really has a target. If it has a target, it is 1, otherwise it is 0. t_i is the position of the needle frame, which is represented by vectors (x,y,w,h), where x and y are the coordinates of the center point of the needle frame, w and h are the width and height of the needle frame, and the dimensions of t_i^* and t_i are the same, indicating the position and size of the real label frame. L_{reg}、L_{reg} represents classification loss and border regression loss respectively. Among them, $L_{\text{reg}}\left(t_i,t_i^*\right)=R\left(t_i-t_i^*\right),R$ represents the smoothL1 loss function. $p_i^* L_{reg}$ represents that the regression loss is calculated only when there is a detection target $\left(p_i^*=1\right)$ in the corresponding needle box, otherwise the regression loss term is 0. p_i and t_i represent the output of classification layer (cls) and border regression layer (reg) respectively. The parameter λ is used to adjust the weight of classification loss and border regression loss. As a rule of thumb, the value of λ is generally set to 10, in which case the weight assigned to the classification layer and the regression layer is identical.

International Water and Irrigation
Volume 43 Issue 2, (2024)
ISSN: 0334-5807
Pages 82 - 96

As shown in Figure 4, rectangular box A and rectangular box B respectively represent the prediction box obtained by the target detection algorithm and the real annotation box in the training data set.

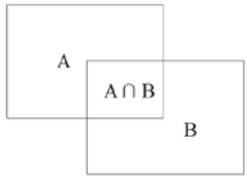

Figure 4 Illustration of IoU definition

IoU represents the overlap rate between prediction box and annotation box, and its calculation formula is as follows:

$$IoU = \frac{A \cap B}{A \cup B} \quad (17)$$

In FasterR-CNN, the position of the prediction box is represented by a four-dimensional vector (x, y, w, h). The area candidate box predicted by the network is represented as $P = \left(P_x, P_y, P_w, P_h\right)$, the manually marked target box is represented as $G = \left(G_x, G_y, G_w, G_h\right)$, and the regression prediction box obtained after border regression is represented as $G^* = \left(G_x^*, G_y^*, G_w^*, G_h^*\right)$.

The essence of border regression is that the network can spontaneously learn a mapping function f, which satisfies $f\left(P_x, P_y, P_w, P_h\right) = \left(G_x^*, G_y^*, G_w^*, G_h^*\right)$, and the regression box $G = \left(G_x^*, G_y^*, G_w^*, G_h^*\right) \approx G = \left(G_x, G_y, G_w, G_h\right)$ is obtained from the original region candidate box after mapping function calculation. That is, the mapped region candidate box P can approach the real annotation box G.

After calculating the region candidate box P through the mapping function F, a regression box G^* can be obtained, and the specific calculation method is as follows:

$$\mathrm{G_x}^* = P_w d_x(p) + P_x \quad (18)$$

$$\mathrm{G_y}^* = P_h d_y(p) + P_y \quad (19)$$

$$\mathrm{G_w}^* = P_w \exp\left(d_w(p)\right) \quad (20)$$

$$\mathrm{G_h}^* = P_h \exp\left(d_h(p)\right) \quad (21)$$

First, the region candidate box P is translated as $(\Delta x, \Delta y)$:

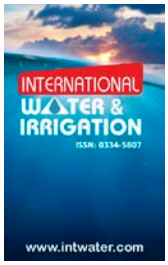

International Water and Irrigation
Volume 43 Issue 2, (2024)
ISSN: 0334-5807
Pages 82 - 96

$$\Delta x = P_w d_w(p), \Delta y = P_h d_y(p) \quad (22)$$

Then, the region candidate box P is scaled:

$$S_w = \exp\left(d_w(p)\right), S_h = \exp\left(d_h(p)\right) \quad (23)$$

By performing the transformation of $d_x(p), d_y(p), d_w(p), d_h(p)$, the border regression can obtain a mapped regression box G^* from the region candidate box P.

The feature vector corresponding to the region candidate frame generated by RPN network is $P = \left(P_x, P_y, P_w, P_h\right)$. After the frame regression, the required offset $d_x(p), d_y(p), d_w(p), d_h(p)$ can be obtained, and then the center coordinate of the region candidate frame is correspondingly translated according to the offset, and the width and height of the region candidate frame are correspondingly scaled, and finally the regression prediction frame obtained is closer to the real labeling frame. It can be seen from the above that P can get the prediction box G^* after being mapped by the function F. In fact, the frame regression should calculate the translation and scale of the region candidate box P, and its corresponding calculation formula is as follows:

$$t_x = \left(G_x - P_x\right) / P_w \quad (24)$$

$$t_y = \left(G_y - P_y\right) / P_h \quad (25)$$

$$t_w = \log\left(G_w / P_w\right) \quad (26)$$

$$t_h = \log\left(G_h / P_h\right) \quad (27)$$

Therefore, the objective function of border regression can be expressed as $d_*(p) = w_*^T \Phi_5(P)$. Among them, w_*^T represents the parameters of the network, $\Phi_5(P)$ represents the feature vectors corresponding to the region candidate boxes, and * represents the position information of the region candidate boxes, that is, four-dimensional vectors (x, y, w, h). The parameter w_*^T of the model are optimized by the least square method, and the final optimization goal is to make $d_*(p)$ approximate the real value $t_* = \left(t_x, t_y, t_w, t_h\right)$, so the loss function of border regression can be expressed as:

$$\text{loss} = \sum_i^N \left(t_*^i - \hat{w}_*^T \Phi_5\left(p^i\right)\right)^2 \quad (28)$$

The formula for the optimization goal of its function is:

International Water and Irrigation
Volume 43 Issue 2, (2024)
ISSN: 0334-5807
Pages 82 - 96

$$w_* = \arg\min_{\hat{w}_*} \sum_{i}^{N} \left(t_*^i - \hat{w}_*^T \Phi_5\left(p^i\right) \right)^2 + \lambda \left\| w_* \right\|^2 \quad (29)$$

In FasterR-CNN, the parameters in the ROI-Pooling pooling layer need to be updated by back propagation. The calculation formula of the ROI-Pooling pooling layer is $y_{rj} = x_i * (r, j)$, in which $x_i * (r, j) = argmax\, x_{i \in R(r,j)}$. $R(r, j)$ is the index values of the output grid after the maximum pooling operation are set, and each x_i corresponds to different output $y_{rj}, x_i \in R$ is the i-th active input of the ROI-Pooling layer, and y_{rj} is the output of the r-th row and j-th column subgrid of the ROI-Pooling layer.

By deducing and calculating the partial derivative of the corresponding loss function after argmax function transformation to each variable x_i, the calculation formula of ROI-Pooling pooling layer back propagation can be obtained, and its formula is as follows:

$$\frac{\partial L}{\partial x_i} = \sum_r \sum_j \left| i = i^*(r, j) \right| \frac{\partial L}{\partial y_{rj}} \quad (30)$$

3 LEISURE SPACE LANDSCAPE DESIGN BASED ON SKETCH LINE SIMULATION

Geometric constraint system refers to the geometric model of leisure space landscape plane and space described by constraints. In the sketch constraint problem, the whole sketch is regarded as a geometric constraint system. It is composed of geometric elements in the sketch and various structural constraints and dimensional constraints added to the geometric elements. After adding constraints between geometric elements or elements themselves, the position and shape changes of geometric elements are obtained by solving geometric constraints, and the geometric elements are rendered in the sketch again. The overall flow chart of the algorithm is shown in Figure 5.

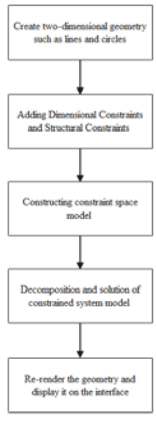

Figure 5 Overall flow of sketch constraint algorithm

International Water and Irrigation
Volume 43 Issue 2, (2024)
ISSN: 0334-5807
Pages 82 - 96

After the structural design of the sketch constraint space model is completed, when the constraints in the sketch change, the constraint space model needs to be maintained. The overall process is shown in Figure 6.

The overall framework of the mechanical three-dimensional scheme construction method based on sketch retrieval is shown in Figure 7, which is composed of the following parts.

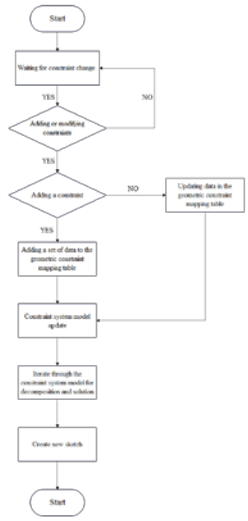

Figure 6 Flow chart of constraint space model

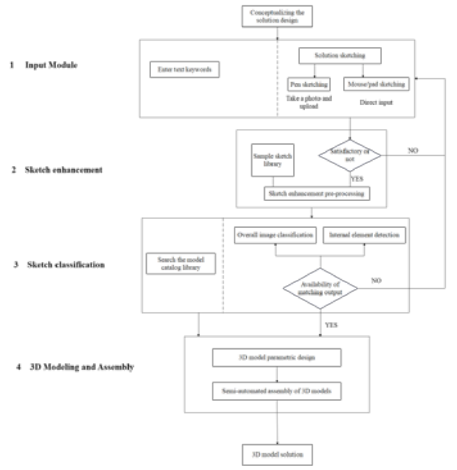

Figure 7 Overall framework of the construction method of leisure space landscape design based on sketch retrieval.

International Water and Irrigation
Volume 43 Issue 2, (2024)
ISSN: 0334-5807
Pages 82 - 96

4 VERIFICATION OF MODEL EFFECT

In this paper, Pytorch deep learning framework is used to implement ResNet network model. In the experiment, the initial learning rate is set to 0.025, and the attenuation is 10 times every 10 cycles. In the training phase, the cross entropy loss is used as the multi-classification loss, and the stochastic gradient descent algorithm with 0.9 momentum is used for optimization. The training process ends after 25 cycles. Figure 8 is a loss monitoring diagram of pre-training on the verification set. Therefore, the pre-training effect is better.

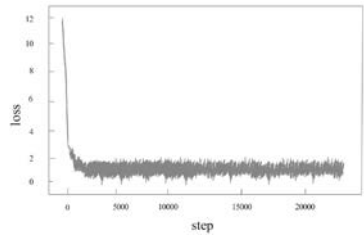

Figure 8 Loss monitoring diagram of pre-training on verification set

In the field of target detection, in order to evaluate the generalization performance of the final detection model, the commonly used evaluation indexes are as follows: Precision, Recall and Mean Average Precision (mAP). The most commonly used is mAP, which can evaluate the detection model more comprehensively, so this paper mainly uses mAP to measure the performance of hand-drawn UI sketch detection model.

(1) Precision: it is also called precision, and represents the ratio of the detected UI sketch components to all detected UI sketch components, and its calculation formula is as follows:

$$\mathrm{Pr}ecision = \frac{TP}{TP + FP} \quad (31)$$

(2) Recall: it is also called recall rate, and represents the ratio of correctly detected UI sketch components to all UI sketch components in the test set. The higher the recall, the less missed sketch components. Its calculation formula is as follows:

$$\mathrm{Re}call = \frac{TP}{TP + TN} \quad (32)$$

(3) mAP: AP is called average precision, which averages the precision at different recall points, and shows the area below the PR curve on the PR curve, as shown in Figure 9. mAP is the average of AP values for multiple categories.

Considering the wide range of size changes of UI sketch components, this paper sets more scale Anchors, which are 32 × 32, 64 × 64, 128 × 128, 256 × 256 and 512 × 512 respectively, and sets the aspect ratio to 1: 1, 1: 2 and 2: 1, so as to generate more diversified scale Anchors. The initial learning rate is set to 0.001, and every 10 epoch is attenuated once, and Batch_Size is set to 2. Before the sketch is input into the network training, the sketch is normalized, and the size of the sketch is adjusted, so that its short side is 800 and its long side is no

International Water and Irrigation
Volume 43 Issue 2, (2024)
ISSN: 0334-5807
Pages 82 - 96

more than 1350. Under different pre-training methods, the change of total loss of FasterR-CNN during training is shown in Figure 10.

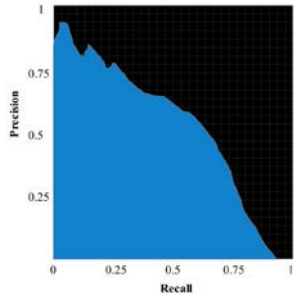

Figure 9 PR Curve

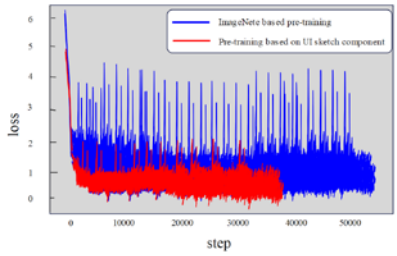

Figure 10 Comparison of total loss of FasterR-CNN under different pre-training methods

As can be seen from fig. 10, the pre-training models under different data sets have different influences on the performance of FasterR-CNN. By pre-training the feature extraction network of FasterR-CNN with UI sketch component data sets, the FasterR-CNN network is easier to converge, faster to converge and lower in total loss in hand-drawn UI sketch detection tasks.

On the basis of the above sketch design, the leisure space landscape design effect verification is carried out. Figure 11 shows the leisure space landscape design effect demonstration. From the figure, it can be seen that sketch line simulation has good effect in leisure space landscape design.

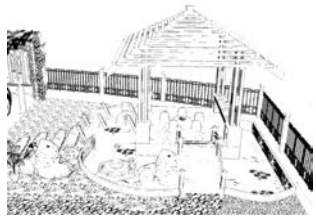

(a) Preliminary draft plans

International Water and Irrigation
Volume 43 Issue 2, (2024)
ISSN: 0334-5807
Pages 82 - 96

(b) Sketch sharpening

(c) Sketch rendering

(d) Preliminary coloring

(e) Final rendering

Figure 11 Demonstration of landscape design effect of leisure space

5 CONCLUSION

Sketches are the concentrated expression of designers' creativity. The premise of creating a good work of art is "knowing fairly well", and sketches can help designers do this to the maximum extent. Nowadays, computers are becoming more and more important tools in various fields of work practice, including design. Moreover, from the design process to the final expression of results, computers play a huge role, and a variety of aided design software are produced accordingly. Their goal is to try to make designers complete the absolute freedom from

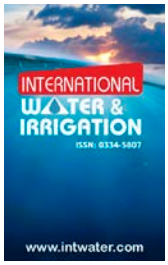

International Water and Irrigation
Volume 43 Issue 2, (2024)
ISSN: 0334-5807
Pages 82 - 96

thinking to expression, but this task was completed by hand-drawn drawings in the past. This paper applies sketch line simulation technology to leisure space landscape design, constructs a design model suitable for modern urban leisure space landscape and analyzes its design effect to improve the scientific nature of leisure landscape design. Through computer simulation research, it can be seen that sketch line simulation has good effect in leisure space landscape design.

ACKNOWLEDGE:

Art Science Planning Project of Heilongjiang Province(Project number:2019D010);

REFERENCES

[1] Ramsey, D., & Malcolm, C. D.: The importance of location and scale in rural and small town tourism product development: The case of the Canadian Fossil Discovery Centre, Manitoba, Canada. The Canadian Geographer/Le Géographe canadien, 62(2), 2018, 250-265.

[2] Drummond, F., & Snowball, J.: Cultural Clusters as a Local Economic Development Strategy in Rural, Small Town Areas: The Sarah Baartman District in South Africa. Bulletin of Geography. Socio-economic Series, 43(43), 2019,107-119.

[3] Abreu, I., Nunes, J. M., & Mesias, F. J.:Can rural development be measured? design and application of a synthetic index to portuguese municipalities. Social Indicators Research, 145(3), 2019,1107-1123.

[4] González Díaz, J. A., Celaya, R., Fernández García, F., Osoro, K., & Rosa García, R.: Dynamics of rural landscapes in marginal areas of northern Spain: Past, present, and future. Land Degradation & Development, 30(2), 2019, 141-150

[5] Pinto-Correia, T., Almeida, M., & Gonzalez, C.: Transition from production to lifestyle farming: new management arrangements in Portuguese small farms. International Journal of Biodiversity Science, Ecosystem Services & Management, 13(2), 2017,136-146.

[6] Yi, Z., Fei, Z., & Ruiqin, L.: The Path of Rural Revitalization in Rapidly Urbanizing Areas: Taking Southern Jiangsu as an Example. China City Planning Review, 27(4), 2018,24-33.

[7] Antic, M., Santic, D., Kašanin-Grubin, M., & Malic, A. : Sustainable rural development in Serbia-relationship between population dynamicss and environment. Journal of Environmental Protection and Ecology, 18(1), 2017, 323-331.

[8] Cecchini, M., Zambon, I., Pontrandolfi, A., Turco, R., Colantoni, A., Mavrakis, A., & Salvati, L. : Urban sprawl and the 'olive'landscape: Sustainable land management for 'crisis' cities. GeoJournal, 84(1), 2019, 237-255.